IEEE Access
Multidisciplinary | Rapid Review | Open Access Journal

IEEE POWER & ENERGY SOCIETY SECTION

Received 22 June 2024, accepted 28 July 2024, date of publication 5 August 2024, date of current version 6 September 2024.

Digital Object Identifier 10.1109/ACCESS.2024.3438881

RESEARCH ARTICLE

Adaptive Droop Gain Control for Optimal Kinetic Energy Extraction From Wind Turbines to Support System Frequency

QIAN CHEN[1], (Student Member, IEEE), LUIS BADESA[2], (Member, IEEE), ZHONGDA CHU[1], (Member, IEEE), AND GORAN STRBAC[1], (Member, IEEE)

[1]Department of Electrical and Electronic Engineering, Imperial College London, SW7 2AZ London, U.K.
[2]School of Industrial Engineering and Design (ETSIDI), Technical University of Madrid (UPM), 28012 Madrid, Spain

Corresponding author: Luis Badesa (luis.badesa@upm.es)

This work was partially supported by MICIU/AEI/10.13039/501100011033 and ERDF/EU under grant PID2023-150401OA-C22.

ABSTRACT Low-inertia power grids would benefit from frequency support from inverter-based generation, given the scarcity of synchronous generators as decarbonisation efforts progress. Wind turbines store kinetic energy in their rotors as they produce electric power, which can be partially released to the grid in the event of a generation loss, in order to contain the frequency drop. This paper introduces a novel fast droop control for wind turbines (WTs) based on an adaptive droop gain strategy, extracting the optimal amount of kinetic energy depending on the overall system conditions. This requires mapping the low-level inverter controls into a system-wide economic optimisation, which has not been successfully addressed yet. To overcome this challenge, we propose a data-driven methodology for integrating frequency stability constraints into an Optimal Power Flow (OPF) formulation, which is explicitly dependent on the low-level control parameters of the wind turbines' converters. A modified Optimal Classification Tree (OCT) is used to encode frequency-security guarantees for the grid, due to its suitable structure for being included in optimisation while maintaining tractability. Through relevant case studies, we demonstrate the effectiveness of the proposed system-aware control for WTs, achieving over 8% system cost savings compared to a system-unaware controller.

INDEX TERMS Frequency stability, data-driven methods, wind turbine controls, convex optimization.

NOMENCLATURE

PARAMETERS OF SECURE OPTIMAL CLASSIFICATION TREE

$\hat{\mathcal{L}}$	Base-line population of the dominant class in the set.
$\mathcal{M}$	big-M value used.
$\mathcal{N}_m^{\text{fea}}$	Maximal number of features combined linearly in branch node m.
Y_i	Class label of observation i (Secure: 1, Insecure: 0).
ϵ	Small value.

INDICES OF SECURE OPTIMAL CLASSIFICATION TREE

i	Observation.
m	Branch node.
t	Leaf node.

SETS OF SECURE OPTIMAL CLASSIFICATION TREE

Ω^J	Features.
$\underline{\Omega}^B$	Branch nodes of global tree.
$\underline{\Omega}^{\mathcal{T}}$	Leaf nodes of global tree.
$\Omega^{\mathcal{N}}$	Training observations.
$\Omega_m^{\mathcal{T}_L}$	Leaf nodes terminating the left branch of node m.
$\Omega_m^{\mathcal{T}_R}$	Leaf nodes terminating the right branch of node m.

CONTINUOUS VARIABLES OF SECURE OPTIMAL CLASSIFICATION TREE

a_m	Contribution vector of features in linear split for branch node m.
n_{1t}	Population of secure observations in leaf node t.
n_{0t}	Population of insecure observations in leaf node t.
l_t	Classification error in leaf node t.

The associate editor coordinating the review of this manuscript and approving it for publication was Feng Wu.

ω Weight of insecure observations in training set $\Omega^{\mathcal{N}}$.
b_m Threshold of splitting condition for branch node m.

BINARY VARIABLES OF SECURE OPTIMAL CLASSIFICATION TREE

d_m 1 if branch node m is built, 0 otherwise.
c_t 1 if class label 1 is assigned to leaf node t, 0 otherwise.
z_{it} 1 if observation i is in leaf node t, 0 otherwise.

I. INTRODUCTION

With the goal of being able to operate the power grid at zero carbon levels by 2025, the Great Britain (GB) electricity system must be able to balance the total national load, operating safely and securely under high instantaneous renewable generation [1]. This ambition demands a step change in the GB power system operation paradigm, from fossil-fuel power dominance to an almost 100% renewable generation in the national grid. Furthermore, the government has planned to deliver on a goal of connecting 50 GW of offshore wind by 2030 [2], which may jeopardise frequency dynamics, since power electronics decouple the physical inertia of wind turbines (WTs) from the grid, thus exacerbating the need for frequency-containment services. In fact, fast frequency support could be delivered by the very WTs, if appropriate controls are put in place.

A. FAST FREQUENCY CONTROL FOR WIND TURBINES

In general, control strategies for fast frequency support (FFS) from variable speed WTs without additional energy storage systems are categorised into two groups [3]. The first group is de-loading control, which operates WTs in a suboptimal mode with a certain amount of reserved power available, to be used in the event of a frequency contingency [4], [5]. Known as overproduction control, the second group is based on providing an additional power injection temporarily from stored kinetic energy [6].

The de-loading control strategy is not preferred for implementation in slightly or even moderate wind-penetrated systems, due to its suboptimal efficiency during normal operation. WT operators may forego important revenues from selling energy, as de-loading implies some power curtailment. Therefore, overproduction control is typically more advantageous, since WTs are enabled to operate following a maximum-power-point-tracking (MPPT) curve under normal conditions [7]. However, several issues may arise from overproduction control, such as a second frequency dip (SFD) and over-deceleration [6], [8].

Overproduction control resorts to the available kinetic energy (KE) stored in WTs, which depends on the pre-disturbance rotor speed and the minimum permissible rotor speed that ensures the mechanical stability of WTs [8]. A temporary overproduction of the power delivered to the grid results in a deceleration of the rotor speed, which drives the operating points of WTs away from the MPPT curve, leading to a lower conversion efficiency of wind power. To regain the maximal power capture and the frequency regulation capability to tackle consecutive under-frequency events, a recovery process of WT's rotor speed is necessary. The rotor speed recovery may entail an output power drop of WTs following the KE extraction process, possibly giving rise to an SFD [9].

Based on the foregoing analysis, to lessen or even eliminate an SFD, it is indispensable to prevent a large and steep electrical power drop from WTs at the end of a rotor deceleration process, which necessitates a smooth decline of reference power for the WTs. An extensive research effort has been conducted to alleviate or erase the SFD. The minimum rotor speed has been preset considering the rate of change of mechanical power versus rotor speed to prevent large power drops [10]. Several shaping functions of the power drop curve have been proposed in [6] to retard a large power drop at the end of the frequency-support period.

On the other hand, several ameliorative strategies have been put forward to avoid an over-deceleration of WTs during the frequency-supporting process. In [11], the WT's post-fault power output trajectory has been devised with significant attention on the chosen rotor speed at the beginning of rotor speed restoration of WTs. Reference [12] has proposed a scheme by navigating the electrical power output of WTs as a specified Gaussian distribution trajectory controlled by the computed standard deviation values, which guarantees the declining rotor speed strictly larger than the minimum permissible rotor speed. The authors in [8] and [13] employed an adaptive droop gain (ADG) in the control loop, which is temporally proportional to the KE stored in WTs to improve the frequency nadir (FN) without the possibility of an over-deceleration. Notably, ADG serves as a function of the WTs' real-time rotor speed and/or Rate of Change of Frequency (RoCoF) of the system to maximise the frequency-supporting capability.

B. OPTIMAL FFS FROM A SYSTEM PERSPECTIVE

The aforementioned approaches focused on the improvement of frequency dynamics on a device level, instead of the aggregate performance of WTs within a wind farm (WF). FFS from WTs should be optimised on a system level, considering the combined response of a number of WTs, since the optimal performance for a single WT does not necessarily correspond to the best solution for the entire power system [14]. Therefore, it is necessary to determine, on a system level, the optimal frequency support from WFs while considering the actual dynamic conditions for individual WTs.

A few papers have addressed the issue of how to optimise FFS from WTs from a system perspective. The authors in [15] and [16] utilised the gain scheduling approach, namely a population of parameter settings in dynamic simulations with a variety of system conditions. Reference [15] argues that the synthetic inertia (SI) control can be viably reduced to

TABLE 1. Summary of control schemes for FFS from WTs.

Ref.	Preventing WT's over-deceleration	Lessening/Eliminating SFDs	Optimised on system level	Benefiting system operational cost
[4]	✓ [1]	✓	✗ [2]	✗
[5]	✓	✓	✗	✗
[7]	✗	✓	✓	✗
[8]	✓	✗	✗	✗
[10]	✓	✓	✗	✗
[11]	✓	✓	✗	✗
[12]	✓	✗	✗	✗
[13]	✓	✗	✗	✗
[15]	✗	✗	✓	✗
[16]	✗	✓	✓	✓
[17]	✗	✓	✓	✓

[1] '✓' indicates the inclusion of the technique in the paper.
[2] '✗' indicates the non-inclusion.

a fast droop control (FDC), where the droop gain is tuned depending on the specific configuration of the power system. In [16], the authors have explored the best performance of FFS from WTs from a system perspective, which is jointly evaluated by the improvement of the FN, the recovery time of frequency response and the presence of an SFD.

However, few previous works have placed this problem within a framework of system scheduling. While the work in [17] demonstrated the significant economic benefits of FFS from WFs, highlighting the added economic value of dynamically optimising this FFS service, the detailed dynamics of WTs were not incorporated into the unit commitment model. This issue was addressed in [7], where the SI provision from WTs was optimised in a unit commitment model, by using analytical system-frequency constraints considering the detailed dynamics of WTs. Table 1 has synthesized the preceding papers from the technical perspectives: preventing WT's over-deceleration, lessening/eliminating SFDs, optimised on system level and benefiting system operational cost. However, our proposed method has accounted for all these techniques, which will be demonstrated in the following contents.

C. MODELLING APPROACHES FOR SYSTEM FREQUENCY SECURITY

In order to optimise the volumes of different frequency-supporting services in an economic setting, security rules are needed that describe the safe region for frequency stability. These rules can then be included as constraints in an economic optimisation model. The state-of-the-art approaches to formulating frequency constraints within system scheduling models can be classified into two groups, i.e. analytical approaches using the swing equation and data-driven approaches based on a time-domain model.

Analytical approaches either model the distinct frequency support services as a set of ramp functions with different slopes and time delays [18], [19], or obtain an analytical expression of frequency deviation based on a multi-machine system frequency response model [20] or an equivalent aggregate system frequency response model [21]. Nevertheless, analytical approaches sacrifice some detail in modelling system frequency dynamics, as it is necessary to forego some accuracy in modelling the primary frequency response to derive closed-form expressions for frequency limits. In all these works, the frequency nadir constraint is nonlinear, with squared terms [18] or square roots [20]. Extensive linearisation techniques have been used to integrate the frequency nadir constraint into a conventional unit commitment problem formulated as Mixed-Integer Linear Programming (MILP) [22], [23], [24], [25]. It should be noted that modelling the frequency response of WTs and synchronous generators (SGs) with standard high-order IEEE models renders deducing linear frequency-security constraints well nigh impossible.

In order to accurately describe the dynamics of FFS from WTs alongside SGs, detailed dynamic models of these assets are expected to be introduced in a system scheduling framework, which is the main incentive behind data-driven approaches for deducing power system security rules. In essence, intelligent data-driven approaches deliver such models with fast and accurate online predicting capabilities, which describe the mapping relationship between the power system operating conditions (input) and the corresponding security status (output) [26]. It should be recognised that the underlying properties of power systems are directly reflected in the data-driven models which only focus on system security attributes and the most relevant features, which obviates the need for complicated model-based analysis without losing any information on dynamics.

Several classifiers have been adopted to represent system security rules for preventive and corrective control, for instance, decision trees (DTs) [27], [28], [29], artificial neural networks (ANNs) [30], [31], [32], deep learning [33], [34], Support Vector Machine (SVM) [35], [36] and logistic regression [37]. ANNs with their rapid computational speed and robust generalisation capabilities, have found

applications in diverse power system challenges, particularly where model-based fall short in delivering the desired levels of accuracy and efficiency. In SVM, the linear technique involves finding a hyperplane that best separates the classes in the input space, which leverages the principle of structural risk minimization, reducing the need for extensive training samples. Deep learning has surpassed traditional machine learning methods and integrated seamlessly into research and industry, demonstrating the ability to autonomously extract valuable features for various tasks. These approaches have been proven effective for data-centric security evaluations of large power systems.

Given the nonlinear and nonconvex frequency security boundary in a high-dimension space, SVM and logistic regression are limited by a hyperplane that simply divides the space into two regions, leading to poor accuracy. In addition, interpretability is of great importance for power system operators, as trust in these classifiers is based on the level of understanding of their predicting processes [26]. Tree models with desired interpretability are advantageous over other methods that perform better in predicting, but are less interpretable. Compared with conventional DT models, Optimal Classification Trees (OCTs) maintain a simple tree structure with lower depth without losing prediction accuracy [29]. Thus, OCT helps to achieve a balance between predictive accuracy and interpretability. Besides, as opposed to neutral networks, OCT with a concise structure ensures tractability of the economic optimisation by introducing significantly fewer binary variables, which is highly desirable for online system-wide economic models. An OCT model has been deployed in [38] for extraction of linear frequency constraints, in which a detailed dynamic model is used for data generation.

D. PRESENT WORK

Given this context, this paper intends to bridge the gap between the device-level converter control and the system-level optimal economic scheduling. An ADG control is proposed to fully utilise the frequency-supporting capability of WFs, while the ADG parameter is introduced as a decision variable in the data-driven frequency-security constraints, and optimised within a system scheduling framework. The main contributions of this paper are threefold:

1) A novel adaptive droop control for wind turbines to support frequency drops is proposed, where the optimal amount of kinetic energy can be extracted from the power system perspective. The ADG is formulated as a function of the electricity grid's operating condition, such as the overall level of reserve, while fully accounting for the dynamics of individual wind turbines.
2) The proposed ADG control framework is further incorporated into the system-level economic optimisation model through a data-driven method, using a tractable and transparent 'fully-secure' OCT formulation. The control parameters of wind turbines are allowed to be explicitly considered as decision variables, while guaranteeing that frequency stability is maintained in every instance.
3) Relevant case studies on an IEEE benchmark network demonstrate that our proposed system-aware control strategy leads to system savings of more than 8%, compared to a system-unaware controller.

The rest of this paper is organised as follows. Section II presents the model of variable speed WT considered and the proposed adaptive droop control. The Secure OCT and the Optimal Power Flow (OPF) formulations are stated in Section III. The results of several case studies implemented in both dynamic simulation and system scheduling frameworks, together with the corresponding analysis and discussion, are included in Section IV. Finally, Section V gives the conclusion.

II. ADAPTIVE FAST DROOP CONTROL STRATEGY

Variable speed WTs are the focus of the ADG control proposed in this paper. This section offers an overview of the variable speed WT model used and the proposed FDC strategy, which is applicable to both doubly fed induction generator (DFIG)-based and permanent magnet synchronous generator (PMSG)-based WT systems.

A. MODEL FOR VARIABLE SPEED WT SYSTEM

Able to operate under a wide range of wind speeds, variable speed WTs are capable of achieving maximum energy conversion efficiency by regulating the rotor speeds dynamically to maintain an optimal tip speed ratio λ, i.e. the ratio of the blade tip speed to the wind speed. The energy conversion efficiency, from available wind power to captured mechanical power, can be expressed as a power coefficient C_p, which is a function of both pitch angle β and tip speed ratio λ. Hence, the mechanical power captured by WTs is described as follows [39]:

$$P_m = \frac{1}{2}\,\rho\,\pi\,R^2\,v_w^3\,C_p(\lambda,\beta) \tag{1}$$

with air density ρ, turbine radius R and wind speed v_w. Without loss of generality, we use here the coefficients for $C_p(\lambda,\beta)$ described in [39]:

$$C_p(\lambda,\beta) = 0.5176\left(\frac{116}{\lambda_i} - 0.4\beta - 5\right)e^{-\frac{21}{\lambda_i}} + 0.0068\lambda \tag{2}$$

with

$$\frac{1}{\lambda_i} = \frac{1}{\lambda + 0.08\beta} - \frac{0.035}{\beta^3 + 1} \tag{3}$$

$$\lambda = \frac{w_r R}{v_w} \tag{4}$$

where w_r denotes the rotor speed of WTs.

For the typical control schemes of DFIG-based and PMSG-based WT systems, the active power output of

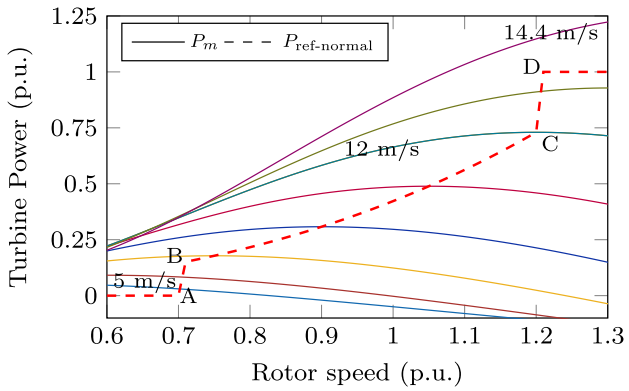

FIGURE 1. Turbine power characteristics (pitch angle $\beta = 0°$).

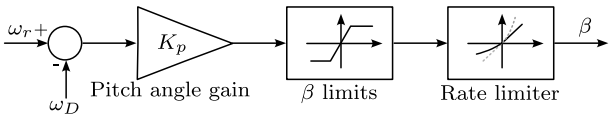

FIGURE 2. Pitch angle control system.

WTs is dictated by the pre-defined power-speed tracking characteristic, namely the active power reference in normal operation $P_{\text{ref-normal}}$ for the rotor-side converter [40]. Such characteristic curve is illustrated in Fig. 1 by the A-B-C-D superimposed curve, and $P_{\text{ref-normal}}$ can be expressed in per unit (p.u.) as follows:

$$P_{\text{ref-normal}} = \begin{cases} 0 & 0 \le w_r < w_A \\ \dfrac{P_B - P_A}{w_B - w_A}(w_r - w_B) + P_B & w_A \le w_r < w_B \\ k_{\text{opt}} \cdot (w_r / w_b)^3 & w_B \le w_r < w_C \\ \dfrac{P_D - P_C}{w_D - w_C}(w_r - w_D) + P_D & w_C \le w_r < w_D \\ P_{\max} & w_D \le w_r \end{cases} \tag{5}$$

where $P_{\text{ref-normal}}$ is in p.u. of nominal mechanical power while w_r is in p.u. of generator synchronous speed, with w_{base} as the base rotational speed.

It should be noted that, under MPPT operation (i.e. B-C curve in Fig. 1), $C_{p-\max}$ can be achieved by maintaining $\lambda = \lambda_{\text{opt}}$ and $\beta = 0°$, i.e. $C_{p-\max} = C_p(\lambda_{\text{opt}}, 0)$. Therefore, differentiating (2) with respect to λ, in order to obtain the value of $C_{p-\max} = 0.48$, the value of $\lambda_{\text{opt}} = 8.1$ is calculated as the maximum. Furthermore, P_C is the maximal power at the base wind speed with $\beta = 0°$. In the pitch angle control system, depicted in Fig. 2, the pitch angle β remains zero degrees until the WTs' rotor speed w_r reaches point D, otherwise it is proportional to the speed deviation from point D.

The specific numerical parameters of the WT model used in this paper are shown in Table 2 [39].

TABLE 2. Parameters of variable speed wind turbine.

Nominal turbine mechanical output power (MW)	1.5
Tracking characteristic speeds [ABCD (p.u.)]	[0.7 0.71 1.2 1.21]
Wind speed at point C (m/s), base rotor speed w_b (p.u.)	12, 1.2
Optimal power gain [k_{opt}]	0.73
Tracking characteristic powers [ABCD (p.u.)]	[0 0.15 0.73 1.0]
Pitch angle controller gain [K_p]	500
Max. pitch angle (deg)	45
Max. rate of change of pitch angle (deg/s)	2

B. PROPOSED ADAPTIVE FAST DROOP CONTROL

The conventional overproduction control for WTs replicates the natural inertial and governor response of SGs via two control loops, i.e. the RoCoF and droop loops. However, differentiating the noise components blended with the measured frequency signal induces large variations of power signal in the RoCoF loop, which accounts for intense torque pulsations in the drive-train of WTs [15]. The pure-droop control (i.e. droop loop only, with no RoCoF loop) accordingly becomes a viable alternative for overproduction control based on the case studies implemented in [15], where the optimal droop gain should notably be tuned dependently on the specific power system characteristics.

Nonetheless, the work in [15] did not consider the issue of WTs' potential over-deceleration during FFS provision. To address this issue, [41] proposes an ADG that is proportional to the real-time kinetic energy stored in the rotor of WTs: At the beginning of frequency falls, a WT with a larger rotor speed thus a larger stored KE is initially set with a larger ADG, while ADG decreases with a declining rotor speed in the subsequent process of KE extraction. A WT stops releasing their KE when the rotor speed w_r declines to the minimum permissible rotor speed $w_{r,\min}$ because ADG is zero. Otherwise, it can lead to over-deceleration in WT generators with limited KE for a large but fixed droop gain. Additionally, if wind speed drops during inertial control, a low gain may even cause over-deceleration. The function of the ADG is given as:

$$\text{ADG}(w_r) = K \cdot (w_r^2 - w_{r,\min}^2) \tag{6}$$

with a fixed constant K. The authors in [8] underscore that design purposes determine the value of K, i.e. this value depends on the power system under consideration. In [40], K has been devised as a function of the wind penetration level 'pl', that is:

$$\text{ADG}(pl, w_r) = K(pl) \cdot (w_r^2 - w_{r,\min}^2) \tag{7}$$

Here K serves as a function of pl to account for the impact of wind penetration level on the aggregated FFS from WFs and hence the post-event frequency evolution. However, a large value of K possibly gives rise to an SFD at large wind speeds, which will be demonstrated in Section IV-A. Moreover, optimal scheduling of the frequency ancillary service of WFs entails information on the system's overall

reserve determined by dispatches of other generation sources, which is not considered in (7).

Accordingly, we put forward the idea that the ADG may simultaneously consider the stable operation of individual WTs and 'optimal scheduling' for FFS from WFs. Furthermore, the 'optimal scheduling' relies on the 'optimal ADG' that renders the system post-fault frequency response respecting the security limits at the minimal operation cost of the power system, which will be illustrated in Section IV-A1. Consequently, our proposed ADG is formulated as an explicit function of WTs' real-time dynamic conditions (i.e. the real-time rotor speed w_r which can be readily measured by encoders in generators) and an implicit function of system-wide operating conditions, i.e. (9), that includes the wind speed v_w, the SGs' dispatches $\boldsymbol{P_G}$, the load levels L_D, the wind penetration level pl and the magnitude of the largest potential power loss ΔP_L. Note that the bold script for $\boldsymbol{P_G}$ means that it is a vector containing the pre-fault dispatches of all the SGs in the system. The proposed function for the ADG can be formulated as:

$$\mathrm{ADG}(v_w, \boldsymbol{P_G}, L_D, pl, \Delta P_L, w_r) = \widetilde{K}_{\mathrm{sys}} \cdot \underbrace{(w_r^2 - w_{r,\min}^2)}_{\text{deter over-deceleration}} \tag{8}$$

with

$$\widetilde{K}_{\mathrm{sys}} = f(v_w, \boldsymbol{P_G}, L_D, pl, \Delta P_L) \tag{9}$$

The 'optimal ADG' resorts to 'optimal $\widetilde{K}_{sys}$' in (8) for achieving the 'optimal scheduling' of FFS from WFs. The mapping relationship between the 'optimal K_{sys}' and the system-wide conditions can be implicitly determined by solving system economic optimisation integrated with frequency stability constraints where $\widetilde{K}_{sys}$ serves as a decision variable. Note that the previously proposed analytical methods for frequency security listed in Section I cannot provide closed-form constraints when $\widetilde{K}_{\mathrm{sys}}$ is modelled as a decision variable, especially considering all the arguments in the ADG included in (9). Therefore, the enhanced ADG control proposed here necessitates a data-driven method for being incorporated into a system-wide economic optimisation, which is another critical novelty of this work. The economic optimisation minimises the system's operational cost given the equality and inequality constraints:

$$\min \ \boldsymbol{c_m}^T \boldsymbol{P_G} \tag{10a}$$

$$\text{s.t. } g(\boldsymbol{x}) = 0 \tag{10b}$$

$$h(\boldsymbol{x}, \widetilde{K}_{\mathrm{sys}}) \le 0 \tag{10c}$$

with the marginal cost of generating units $\boldsymbol{c_m}$ and $\boldsymbol{x}$ serves as a vector of steady-state decision variables of power systems, including active/reactive powers of generators and nodal voltage magnitudes/phase angles. (10b) are power balance equations in all nodes, while (10c) involve post-fault frequency stability constraints and a set of operational constraints considering branch flow limitations, generator

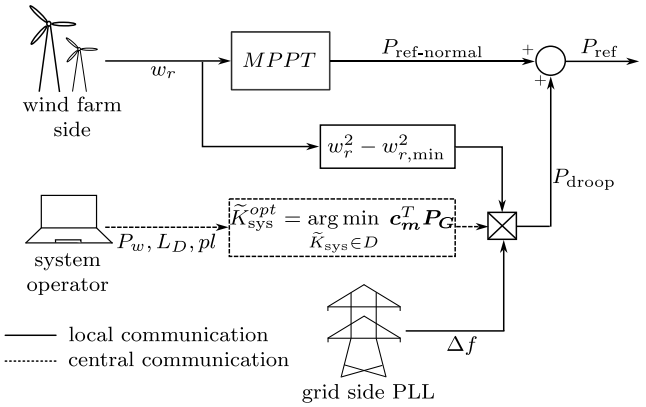

FIGURE 3. Control scheme for the proposed adaptive droop gain.

capacities and nodal voltage limits. Note that $\widetilde{K}_{\mathrm{sys}}$ would only appear in the inequality constraints which are in the form of (13). Hence, the 'optimal $\widetilde{K}_{\mathrm{sys}}$' can be expressed as:

$$\widetilde{K}_{\mathrm{sys}}^{opt} = \underset{\widetilde{K}_{\mathrm{sys}} \in D}{\arg\min} \ \boldsymbol{c_m}^T \boldsymbol{P_G} \tag{11}$$

where D is the feasible region defined by (10b) and (10c). The proposed strategy of adaptive FDC is presented in Fig. 3. It is achievable to attain the 'optimal ADG' in local WF systems through hourly updating by the system operator based on communication networks: the system operator needs to provide the local droop controller in WFs with hourly system-wide information, such as the wind penetration level and the predicted wind power and load. The real-time information, i.e. rotor speed measured from WTs' side and local frequency excursion measured by a phase-locked loop (PLL) connected to the grid, are delivered to the local controller as well. Note that P_w is the available wind power, as defined by the wind speed v_w in (5).

The proposed FDC strategy is remarkably applicable to both DFIG-based and PMSG-based WT systems with their rotor-side converters (RSCs) in power control: Under their grid-side converters (GSCs) oriented to the grid, the power command for RSCs, i.e. P_{ref} in Fig. 3, comes from the WT control centre to realize MPPT in normal cases or FFS in frequency contingencies. More precisely, the RSCs in back-to-back converters of both systems attempt to deliver their desirable active powers to grids by regulating the rotor speeds. However, the power flow in the rotor circuit for DFIG is bidirectional depending on the rotor speed compared with the synchronous speed of the grid, while PMSG constantly works in synchronous mode with unidirectional power flow in converters.

III. FREQUENCY-SECURED SYSTEM OPERATION VIA DATA-DRIVEN CONSTRAINTS

Here we present the proposed frequency-secured economic dispatch methodology. The problem is formulated as an OPF with frequency-limits constraints, where we introduce an improved OCT approach for power system

frequency security, incorporating the optimal ADG control presented before.

A. MULTIVARIATE OPTIMAL CLASSIFICATION TREE WITH FREQUENCY-SECURITY GUARANTEES

A multivariate optimal classification tree encoding the frequency-security guarantees (referred to as 'Secure OCT(M)') is formulated in this section as a mixed-integer optimisation problem. This is an enhanced formulation proposed in this paper, based on the OCT(M) approach introduced in [29], to remove the 'false safe' predictions. This is achieved by modifying the cost function in the OCT(M) model.

Given that the electricity grid is a safety-critical system, and that uncontrolled frequency decline could potentially lead to system collapse, this modified OCT(M) removes any 'false safe' predictions, as these correspond to 'unsafe' scenarios predicted as 'safe' operating points. In turn, removing 'false safe' predictions implies increasing the conservativeness of the tree, as will be discussed later. The proposed loss function in the Secure OCT(M) and associated constraints are formulated as follows. The remaining OCT(M) constraints are not included for conciseness, the interested reader can refer to [29].

$$\min \frac{1}{\hat{\mathcal{L}}} \sum_{t \in \underline{\Omega}^{\mathcal{T}}} l_t + \alpha \sum_{m \in \underline{\Omega}^{B}} d_m \tag{12a}$$

$$\text{s.t. } l_t \geq \omega \cdot n_{0t} - \mathcal{M} \cdot (1 - c_t) \quad \forall t \in \underline{\Omega}^{\mathcal{T}} \tag{12b}$$

$$l_t \leq \omega \cdot n_{0t} + \mathcal{M} \cdot c_t \quad \forall t \in \underline{\Omega}^{\mathcal{T}} \tag{12c}$$

$$l_t \geq n_{1t} - \mathcal{M} \cdot c_t \quad \forall t \in \underline{\Omega}^{\mathcal{T}} \tag{12d}$$

$$l_t \leq n_{1t} + \mathcal{M} \cdot (1 - c_t) \quad \forall t \in \underline{\Omega}^{\mathcal{T}} \tag{12e}$$

$$n_{1t} = \sum_{i \in \Omega^{\mathcal{N}}} z_{it} \cdot Y_i \quad \forall t \in \underline{\Omega}^{\mathcal{T}} \tag{12f}$$

$$n_{0t} = \sum_{i \in \Omega^{\mathcal{N}}} z_{it} - n_{1t} \quad \forall t \in \underline{\Omega}^{\mathcal{T}} \tag{12g}$$

The objective function (12a) aims to minimise the misclassification cost and maintain a simple tree structure as far as possible. More precisely, the first item in (12a) accounts for the total classification error in all candidate leaf nodes, and the second term penalises the number of branch nodes in the global tree. Parameter $\hat{\mathcal{L}}$ is a baseline value of misclassification error for the entire, i.e. the sample number of the minor class, while α is a complexity parameter for regulating the split number of a tree model and the detailed tuning procedures have been presented in [42].

The binary variable z_{it} is introduced to track if data point i is assigned to leaf node t. The number of observations labelled with class 1 in each leaf node, denoted as n_{1t}, is calculated in (12f) with the parameter $Y_i = 1$ for 'safe' observations. Accordingly, $Y_i = 0$ accounts for 'unsafe' data points, used to calculate the number of observations with class 0 for each leaf node in (12g). Decision variable c_t is used to track the prediction of each terminal node: $c_t = 1$ denotes

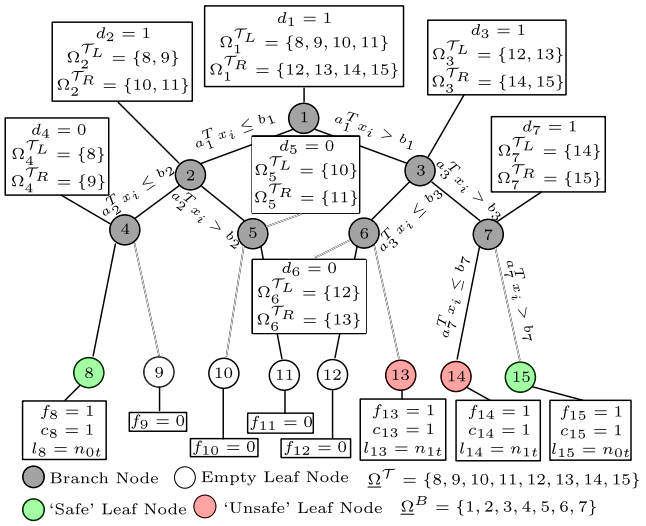

FIGURE 4. Demonstration model of multivariate OCT.

that leaf node t predicts unseen observations as secure cases (corresponding to class 1), while $c_t = 0$ corresponds to the insecure class. The big-M constraints (12d) and (12e) enforce the misclassification cost $l_t = n_{1t}$ if terminal node t corresponds to class 0. Constraints (12b) and (12c) enforce $l_t = n_{0t}$ if $\omega = 1$ with leaf node t assigned to 'safe' class ($c_t = 1$), while values of $\omega > 1$ allow increasing the weight of unsafe operating points; these constraints are instrumental to predicting 'unsafe' points, i.e. eliminating 'false safe' predictions.

We define the optimal ω as ω^*: The full precision of the trained model with ω^* can be evaluated on the validation set with the maximal accuracy achieved. A complete tuning process for identifying ω^* that would eliminate 'false safe' predictions follows:

1) Tune all the hyper-parameters in Secure OCT with $\omega = 1$ based on the validation set.
2) Use the grid-search technique, i.e. parameter sweep through a manually specified subset, to find ω_0 from the CART model with the same hyper-parameters in Step 1 so that the maximal accuracy can be obtained without losing any precision.
3) Inject the CART solution and ω_0 as a warm start to the Secure OCT model for training.
4) Test the precision on the validation set based on the trained OCT model: if the precision is not 100%, increase ω from ω_0 to obtain ω^*. Otherwise, decrease ω to ω^* until the precision starts to decrease.

To exhibit the mathematical structure for encoding frequency-security guarantees, an OCT(M) is shown in Fig. 4 to give further insight into the integer programming. The splitting characteristic of branch nodes are dictated by the binary variable d_m: branch nodes 1, 3, 7 are built with their $d_m = 1$ while no splits are performed in nodes 2, 4, 5, 6 ($d_m = 0$). Furthermore, the OCT formulation restricts a branch node from applying a split if its parent node does

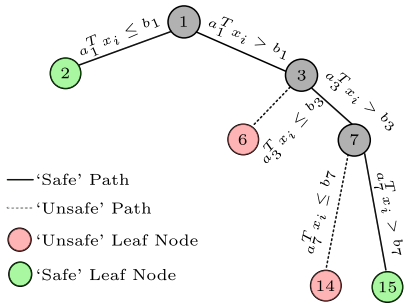

FIGURE 5. Concise equivalent model for multivariate OCT demonstration.

not perform a split. For example, in Fig. 4, no splits are in node 4, 5 as no split is applied in node 2. Hence, leaf node 8 contains the same set of observations as branch node 2 given no splitting in nodes 2 and 4, i.e. $d_2 = 0$ and $d_4 = 0$. The same situation is applied to branch node 6 and leaf node 13. Therefore, no observations are located in branch node 5 and leaf nodes 9, 10, 11 and 12, leading to $f_t = 0$ for $t \in \{9, 10, 11, 12\}$. The concise structure of the OCT model has been reduced based on Fig. 4 by pruning the redundant nodes and branches and shown in Fig. 5 to help readers understand better.

Branch node m splits the training set by $a_m^T x_i \leq b_m$ and $a_m^T x_i > b_m$, and they are followed by leaf node $t \in \Omega_m^{\mathcal{T}_L}$ terminating in the left branch of m and leaf node $t \in \Omega_m^{\mathcal{T}_R}$ terminating in the right branch of m respectively. The binary variable f_t indicates whether leaf node t is empty ($f_t = 0$) or not ($f_t = 1$). Given the limited numerical precision in MIP solvers, non-strict constraints $b_m + \epsilon - a_m^T x_i \leq 0$ are changed from inequality ones $a_m^T x_i > b_m$ in the course of integer programming. We need to introduce a binary variable p_m to track the 'safe' path in the tree which threads the critical branch nodes $m \in \underline{\Omega}^B$. The critical branch nodes in Fig. 4 are $m = \{1, 3, 7\}$. We specify that $p_m = 0$ implies $a_m^T x_i \leq b_m$ while $p_m = 1$ forces $b_m + \epsilon - a_m^T x_i \leq 0$ to be activated using big-M strategy. Hence, the mathematical structure for encoding frequency-security guarantees is presented here:

$$a_1^T x_i - b_1 \leq \mathcal{M} \cdot p_1 \tag{13a}$$
$$(b_1 + \epsilon) - a_1^T x_i \leq \mathcal{M} \cdot (1 - p_1) \tag{13b}$$
$$(b_3 + \epsilon) - a_3^T x_i \leq \mathcal{M} \cdot (1 - p_3) \tag{13c}$$
$$p_1 \leq p_3 \leq p_1 \tag{13d}$$
$$(b_7 + \epsilon) - a_7^T x_i \leq \mathcal{M} \cdot (1 - p_7) \tag{13e}$$
$$p_3 \leq p_7 \leq p_3 \tag{13f}$$

B. SECOND-ORDER CONE OPF WITH MIXED-INTEGER LINEAR FREQUENCY-SECURITY CONSTRAINTS

Given that the alternating-current OPF problem is nonconvex, several approximations and relaxations have been proposed, such as direct-current (DC)-OPF, Second-Order Cone Programming (SOCP)-OPF and Semidefinite Programming (SDP)-OPF. SOCP-OPF exhibits several merits: on the one hand, it is more general than the linear DC-OPF approximation, allowing to model reactive power within the network; on the other, it is less sensitive to the network scale than the more general SDP-OPF, requiring fewer computational resources [43]. To test our proposed methodology for optimal kinetic energy extraction from WTs from a system-wide perspective, we use here a standard SOCP-OPF formulation such as the one described in [44]. Note however that the ADG strategy for fast frequency support and associated Secure OCT(M) are applicable to other OPF formulations.

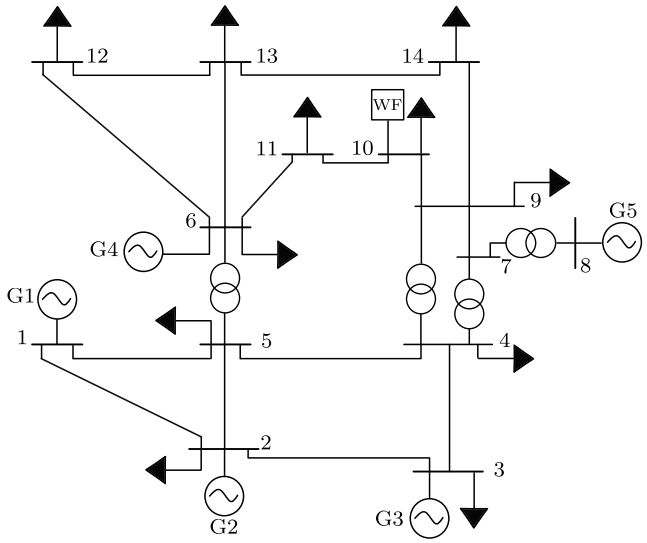

FIGURE 6. IEEE 14-bus test system.

The purpose of SOCP-OPF is to minimise the total generation cost subject to a set of steady-state constraints, such as active and reactive power balance, generation limits, voltage magnitude limits and transmission line limits. We also include the frequency-security constraints accounting for maximum admissible frequency deviation ($\Delta f_{\max} \leq 0.8$ Hz, as per GB standards), maximum admissible RoCoF, $(df/dt)_{\max} \leq 1$ Hz/s, and maximum admissible frequency deviation at quasi-steady-state (q-s-s) ($\Delta f_{\max}^{\text{ss}} \leq 0.5$ Hz) [45].

The frequency-security constraints defined by the Secure OCT(M) model have been encoded within the SCOP-OPF in the pattern demonstrated in (13). The data used for training the Secure OCT(M) model is generated from the detailed dynamic system model implemented in MATLAB/Simulink. In essence, the set of MILP constraints provides an accurate approximation to the highly nonlinear, nonconvex boundary distinguishing the 'safe' and 'unsafe' frequency scenarios in the high-dimensional space, wherein the number of dimensions is in line with the number of data features (i.e., P_w, $\boldsymbol{P_G}$, L_D, pl, ΔP_L, $\widetilde{K}_{\text{sys}}$). The accuracy of the Secure OCT(M) as a frequency-security classifier is analysed in the following section.

IV. CASE STUDIES

Several case studies on a modified IEEE 14-bus system as shown in Fig. 6, implemented with the values from [46],

TABLE 3. Thermal generation mix within test case.

	G1	G2	G3	G4	G5
Number of Units	2	2	1	1	1
Rated Power (MW)	112.5	70	100	95	105
Min Stable Generation (MW)	5	17.5	20	15	25
Governor Droop Gain (%)	N/A	N/A	0.08	0.06	0.05
Max governor response (MW)	N/A	N/A	65	35	70
Rated Reactive Power (Mvar)	10	50	40	24	24
Min Reactive Power (Mvar)	0	-40	0	-6	-6
Cost coefficient c_1 (£/MWh)	50	40	20	30	10
Cost coef. c_2 (£/(MW)^{2}h)	0.5	0.4	0.2	0.3	0.1

are conducted to demonstrate the benefits of the proposed ADG control strategy, where the ADG value is optimised from a system-benefits perspective. Two models are used in this section: 1) a detailed dynamic model used to generate a data set of safe and unsafe operating points regarding frequency stability, which is then used as a training set for the Secure OCT(M); and 2) a frequency-secured MISOCP-OPF model to provide the optimal system dispatch. The full dynamic model is finally used again to validate the dispatch solutions, testing if the potential frequency excursions following the largest contingency would respect the pre-defined frequency limits.

The conventional IEEE type governors like DEGOV1 for diesel generators, IEEEG1 for gas and steam generators, together with AVRs (Automatic Voltage Regulators) such as SEXS for steam units, and GAS and EXST1 for diesel units, describe the dynamic characteristics of the thermal power units [47]. DFIG-based WT system has been employed with optimal torque control for the RSC and the GSC maintaining dc-link voltage and providing reactive power to the grid. In our model, the PLL has served as a grid-synchronisation technique to account for its effects on system frequency response, such as the increasing oscillations and settling time [48]. The characteristics of the thermal units in Fig. 6 are presented in Table 3. Units G1 and G2 are assumed to be unsuitable for primary frequency control, given their slow dynamics. In our simulation, we include a WF in bus 10 modelled as an aggregation of several identical WTs with the same operating conditions. Data for wind and load profiles corresponding to the GB system are used, taken from [49]. The optimisation problem is formulated in MATLAB via the modelling layer YALMIP [50], and calling Gurobi as the solver, with default parameterisation. All simulations were carried out on a standard laptop with AMD Ryzen 7 5800H CPU, with a clock rate of 3.20 GHz and 16 GB of RAM.

A. IMPACT OF SYSTEM-WIDE CONDITIONS ON OPTIMAL $\widetilde{K}_{SYS}$

Several results of the detailed dynamic model, implemented in MATLAB/Simulink, are used here to showcase the dependency of $\widetilde{K}_{\text{sys}}^{\text{opt}}$ on system-wide conditions. As discussed

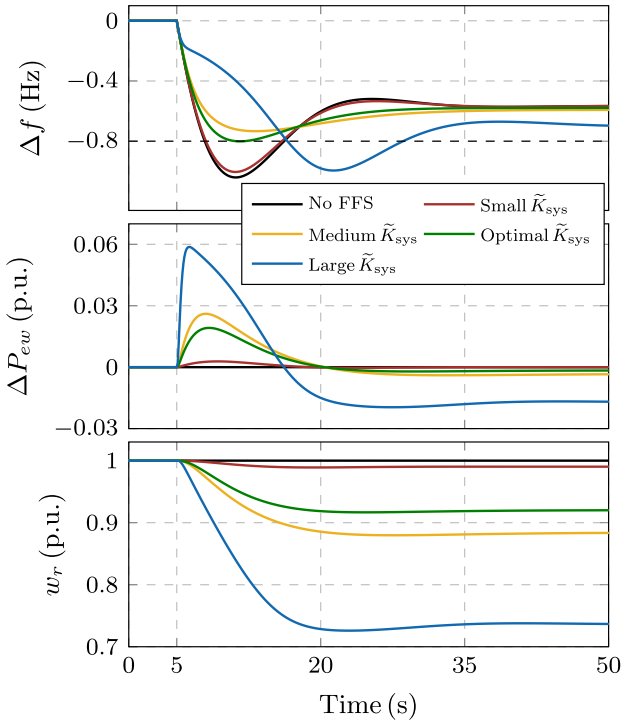

FIGURE 7. Results for Case A-1: (a) System frequency; (b) Active power output of WF; (c) Rotor speed of WTs.

in Section II-B, the optimal $\widetilde{K}_{\text{sys}}$ is such a value that generation cost is minimised on the premise of system frequency security. For clarity in the explanations, we focus on cases where the frequency-nadir limit is the binding constraint (i.e. $\Delta f_{\max} \leq 0.8$ Hz), a typical case in low-inertia systems as demonstrated by [17], [18]. Hence, the optimal $\widetilde{K}_{\text{sys}}$ is such a value that the frequency drop is contained at exactly 0.8 Hz. The contingency under consideration is a generation loss of 5% of the total installed thermal capacity, i.e. $\Delta P_L = 0.05\, C_{\text{SG}}$, where C_{SG} is the total installed capacity of thermal generators in the system.

1) INTERPRETATION OF OPTIMAL $\widetilde{K}_{\text{SYS}}$

We consider a case with $v_w = 10$ m/s and $pl = 20\%$, and include the Center-of-Inertia (CoI) frequency excursions in Fig. 7, where the optimal $\widetilde{K}_{\text{sys}}$ arrests the FN to 0.8 Hz exactly. It is evident that the FN improvement is conditional on the value of $\widetilde{K}_{\text{sys}}$: a small value incurs a poor performance of post-fault frequency response, infringing the frequency security rules. In contrast, despite a medium value raising the FN to a better extent, the generation cost would not be minimum, as containing the FN well above the critical value of 0.8 Hz implies that more headroom than strictly necessary has been scheduled in the thermal generators (with the associated increase in system operation costs). It is noteworthy that a large value of $\widetilde{K}_{\text{sys}}$ instead worsens the FN incurring an SFD, as the electrical power reduces dramatically with the declining rotor speed of DFIG-based WTs, also shown in Fig. 7. The DFIG is operated stably

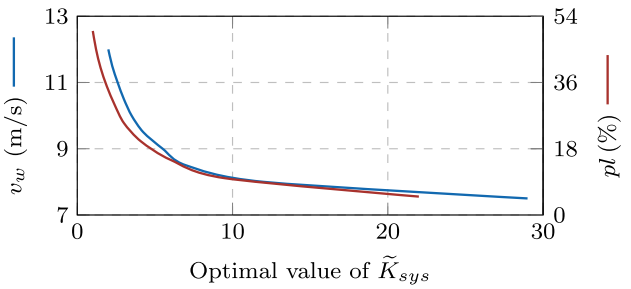

FIGURE 8. Optimal $\widetilde{K}_{\text{sys}}$ versus wind speed and wind penetration level '*pl*'.

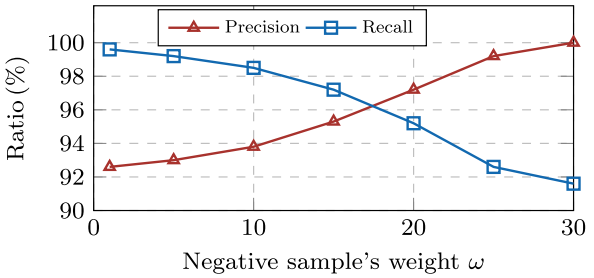

FIGURE 9. Prediction performance versus negative sample's weight ω.

above the minimum permissible rotor speed which is 0.7 p.u., considering DFIG-based WTs' rotors are generally designed to operate from 0.7 p.u. to 1.3 p.u. dynamically.

2) OPTIMAL $\widetilde{K}_{\text{SYS}}$ DEPENDING ON WIND SPEED

With increasing wind speed 'v_w', the results demonstrate that the optimal value of $\widetilde{K}_{\text{sys}}$ follows a monotonically decreasing function, as illustrated in Fig. 8, which was obtained considering again a $pl = 20\%$. This trend can be understood by rewriting (8) to express the initial value of ADG as follows:

$$\begin{aligned}\text{ADG}_0(v_w) &= \widetilde{K}_{\text{sys}} \cdot (w_{r0}^2 - w_{r,\min}^2) \\ &= \widetilde{K}_{\text{sys}} \cdot \left[\left(\frac{\lambda_{\text{opt}} v_w}{R} \right)^2 - w_{r,\min}^2 \right] \\ &= \widetilde{K}_{\text{sys}} \cdot G(v_w) \end{aligned} \tag{14}$$

with the initial rotor speed w_{r0} assuming that WTs are operated in MPPT mode. The monotonically increasing function $G(v_w)$ entails a fall of $\widetilde{K}_{\text{sys}}^{\text{opt}}$ to balance the contribution from growing wind speeds.

3) OPTIMAL $\widetilde{K}_{\text{SYS}}$ VS. WIND PENETRATION LEVEL

It can be clearly seen in Fig. 8 that the penetration level of wind, '*pl*', induces a steep decrease in the optimal value of $\widetilde{K}_{\text{sys}}$, where the results were obtained for a fixed $v_w = 10$ m/s. To better understand this trend, let us consider the definitions of active power increase in the WTs as dictated by the droop control, and of wind penetration level as a ratio of the rated power of the WF to total installed generation capacity:

$$P_{\text{droop}} = \underbrace{\widetilde{K}_{\text{sys}} \cdot (w_r^2 - w_{r,\min}^2) \cdot \Delta f}_{\text{per unit value}} \cdot C_{\text{WF}} \tag{15}$$

$$pl = \frac{C_{\text{WF}}}{C_{\text{WF}} + C_{\text{SG}}} \Rightarrow C_{\text{WF}} = \frac{pl}{1 - pl} \cdot C_{\text{SG}} \tag{16}$$

where C_{WF} corresponds to the rated power of the WF. Substituting (16) into (15) yields:

$$P_{\text{droop}} = \widetilde{K}_{\text{sys}} \cdot (w_r^2 - w_{r,\min}^2) \cdot \Delta f \cdot C_{\text{SG}} \cdot H(pl) \tag{17}$$

with $H(pl) = \frac{pl}{1-pl}$. Therefore, a decline of $\widetilde{K}_{\text{sys}}^{\text{opt}}$ moderates the contribution of $H(pl)$, which is a monotonically increasing function.

B. ASSESSMENT OF CONSERVATIVENESS AND RELIABILITY OF SECURE OCT(M)

As discussed in Section III-A, appropriate tuning of the hyperparameter ω in the Secure OCT(M) is needed to guarantee frequency security in all instances, i.e. achieve full reliability. A larger value of ω implies that the prediction accuracy of the classifier will be reduced to a certain extent, as some 'safe' cases are likely to be misclassified, which is indicative of the conservativeness of the approach. In this section, we employ two metrics, precision and recall, to assess our proposed model's reliability and conservativeness. If 'safe' and 'unsafe' are defined as 'positive' and 'negative' outcomes respectively, a larger number of false-positive observations render a lower precision, i.e., a less reliable model. Likewise, the larger the number of false-negative cases is, the more conservative the model would be, i.e., the lower recall is. In this section, since the weekly wind and demand forecasts were used, a set of 1500 observations has been created as typical samples for a week, using 70% of the overall set for training, 20% as a validation set, and 10% for testing. The effect of different values of ω on the performance of the Secure OCT(M) is illustrated in Fig. 9, which shows a decrease of recall and increment of precision in the studied range of ω. A value of $\omega = 30$ fully mitigates the risk of 'false safe' predictions (100% precision). Regarding computing time, running the dynamic simulations for labelling the 1500 samples (i.e., creating the data set) took roughly two days, while just over 36 min were necessary for training the Secure OCT(M) with $\omega = 30$. The OCT training process involves solving a MILP problem. Using a small training dataset significantly reduces the training time. Consequently, frequency constraints can be updated monthly using small-size training datasets generated from short-term wind and load predictions. This approach ensures that the model stays up-to-date and efficient by continuously incorporating the latest data.

For benchmarking our proposed Secure OCT(M), two other tree methods are considered: conventional decision tree (CART), and OCT(M) in [29]. Table 4 presents the evaluation of the conservativeness and the reliability of these three models on the testing set. The results show that hyperparameter ω in the Secure OCT(M) improves the

TABLE 4. Assessment indices of three classification models.

	Precision (%)	Recall (%)	Depth
Secure OCT(M) ($\omega^* = 30$)	100	91.62	2
OCT(M) in [29]	98.36	98.07	2
CART	86.69	96.65	6

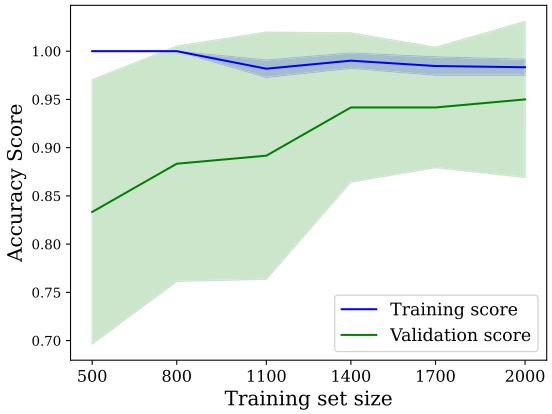

FIGURE 10. Learning curve of OCT(M): relationship between prediction accuracy and training set size.

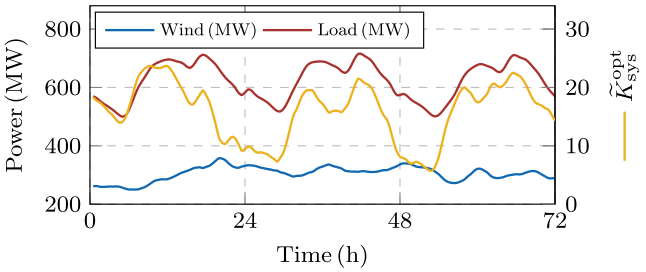

FIGURE 11. Three-day wind and load profiles and optimal $\widetilde{K}_{\text{sys}}$.

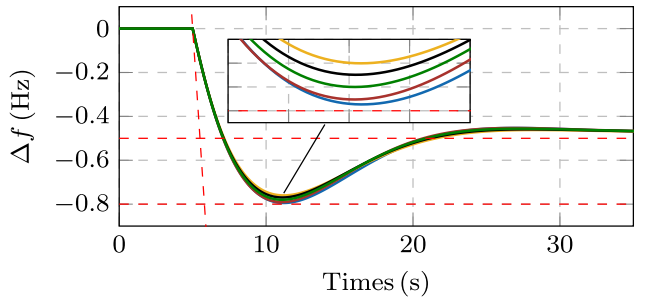

FIGURE 12. Dynamic simulations from five different OPF solutions.

classifier's reliability by erasing false-positive samples by inevitably misclassifying some 'safe' scenarios. Accordingly, our proposed model becomes more conservative but fully reliable, in contrast with the other two tree models.

In addition, OCT challenges the notion that optimal methods merely overfit the training set and fail to generalize effectively. The OCT model has been proven more efficient and robust versus CART in learning the ground truth of data, thus endowed with the adaptability of diverse datasets [42]. The learning curve shown in Fig. 10 represents the learning performance of our proposed OCT model on the training and validation sets as a function of the training set size, where the cross-validation technique has been used. The number of samples used in the training set increases from 500 to 2000. The prediction accuracy serves as the performance metric for both the training score and validation score. To diagnose the accuracy and generalisability of the model, we resort to the concept of bias-variance tradeoff. Bias refers to a measure of how closely a model's predictions match the true outcomes, while variance suggests how much the model's predictions vary when trained on different subsets of the training data. In Fig. 10, the training and validation scores converge to a high accuracy as the number of training samples increases, where high accuracy indicates low bias and convergence implies low variance. Hence, the result suggests that our proposed OCT model is a good fit, i.e. low bias and low variance, which has sufficient capacity to predict and generalize well. Note that Fig. 10 conveys not just the central tendency, i.e. mean scores, but also the variability, i.e. the filled area between the mean scores and the standard deviations, which helps to understand the reliability of the model.

C. VALIDATION OF FREQUENCY-SECURITY CONSTRAINTS

In order to validate the frequency-security constraints defined by the Secure OCT(M), in this section the dispatch solutions from a multiperiod OPF model were fed into the dynamic model in MATLAB/Simulink. The system parameters in the scheduling model were set as follows: load demand $P_D \in [500, 715]$ MW and $pl = 30\%$. The contingency which defines the need for frequency services, ΔP_L, is optimally modelled as the largest single power output at any point in time, therefore this value is co-optimised along with the volume of frequency reserves and $\widetilde{K}_{\text{sys}}$. Fig. 11 displays a set of $\widetilde{K}_{\text{sys}}^{\text{opt}}$ obtained in the course of system scheduling for a three-day profile of load and wind power. It can be seen that the optimal $\widetilde{K}_{\text{sys}}$ fluctuates under the joint effect of wind speeds and pre-fault dispatches of thermal units. Simultaneously, the optimal $\widetilde{K}_{\text{sys}}$ is shown to be inversely proportional to wind power (i.e., wind speed), as demonstrated in Section IV-A2.

Dynamic simulations were run in the Simulink model by feeding the dispatch solution for 5 different half-hour periods, arbitrarily chosen among all dispatch solutions for the three-day period in Fig. 11. The results in Fig. 12 demonstrate that the requirements for RoCoF, FN and q-s-s are respected in all cases, namely $(df/dt)_{\max} \leq 1.0$ Hz/s, $\Delta f_{\max} \leq 0.8$ Hz and $\Delta f_{\max}^{\text{ss}} \leq 0.5$ Hz. The nadir constraint is binding in all five OPF instances, while Fig. 12 shows that in some of these cases the FN does not hit the limit of 0.8 Hz. The trigger for this slight conservativeness in the nadir constraint is the use of the parameter ω in the Secure OCT(M): in order to achieve 100% precision, certain 'safe' observations in the vicinity of the FN limit are misclassified. However, compared with the OCT(M) with

TABLE 5. Frequency nadir assessment.

Linearisation Models	Nadir (Hz)		
	Min	Mean	Max
Secure OCT(M)	0.686	0.735	0.796
OCT(M) in [29]	0.740	0.789	0.823

TABLE 6. Dispatch results under secure vs. Standard OCT(M).

	Total cost (£m)	Reserves (MW)
Secure OCT(M)	69.6	91.65
OCT(M) in [29]	65.6	88.35
Difference	0.6%	6.4%

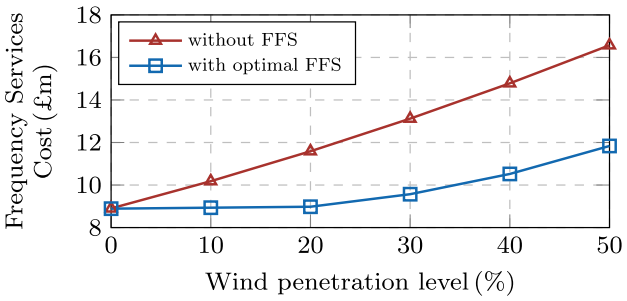

FIGURE 13. Impact of optimal FFS on the weekly cost of frequency services.

no security guarantee, the results in Table 5 demonstrate that the Secure OCT(M) achieves frequency reliability in all instances. This effect is also seen in the average half-hourly frequency reserves dispatched by the OPF, i.e. the average headroom in thermal generators, presented in Table 6: while our proposed method incurs in 6.4% extra reserves compared to the standard OCT(M), this safety margin allows achieving full reliability. The increase in system operating costs due to these extra reserves is of 0.6%, which is the cost of guaranteeing security at all times.

D. IMPACT OF OPTIMAL FFS ON POWER SYSTEM OPERATING COST

The cost of frequency services versus the wind penetration level, ranging from 0 to 50%, is depicted in Fig. 13, considering two scenarios: (1) with optimal FFS; and (2) without optimal FFS. As expected, WTs providing FFS indeed share the burden with thermal units of supporting frequency, which reduces the volume of necessary headroom in SGs compared to the case without optimal FFS, and thus decreases the system cost of frequency services.

Finally, we evaluate the value of optimising $\widetilde{K}_{\text{sys}}^{\text{opt}}$ in terms of system savings. To do this, the weekly operating cost resulting from the OPF is compared with a case where the droop gain is not optimised as a function of the system operating conditions, i.e. the simpler control strategy of fixing the value of K in (8) to a pre-set value. The results for the

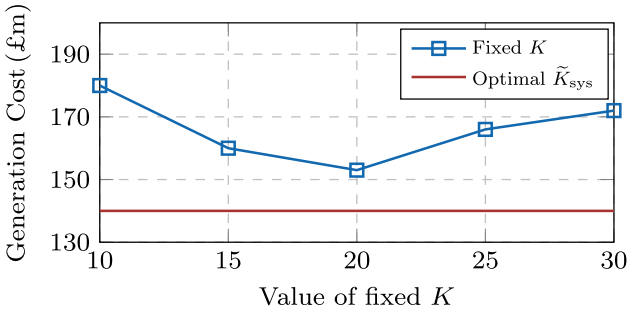

FIGURE 14. Weekly generation cost with different control strategies, for a 50% wind penetration level.

50% wind penetration case are included in Fig. 14, where a range of values for the fixed $K \in [10, 30]$ has been considered. It should be noted that in Fig. 14 the generation cost based on optimal $\widetilde{K}_{\text{sys}}$ is constant, not a function of the value of fixed K. The results in Fig. 14 show that generation cost decreases until $K = 20$, which is driven by the increasing FFS capability of WTs. After that point, the underproduction process of WTs triggers the growth of generation cost, as discussed in Section IV-A. It is clear that dynamically optimising $\widetilde{K}_{\text{sys}}$ significantly outperforms the 'fixed K strategy', leading to a minimal reduction of around 8% in system operating cost, which is calculated at $K = 20$ (implying that this is the optimal value in the set of 'fixed K' candidates). Furthermore, it is important to point out that the optimal value of fixed K can only be obtained by incorporating the fixed WT droop control into economic optimisation through the proposed data-driven method. This value of $K = 20$ could not be computed using previously proposed models, thus highlighting the benefit of the proposed framework.

V. CONCLUSION AND FUTURE WORK

This paper proposes a fast droop control for WTs via an adaptive droop gain. The gain is optimised to maximise system-wide economic savings, using an OPF model with frequency-security constraints that are extracted from a detailed dynamic power system model. This is achieved by resorting to a data-driven method based on a revised optimal classification tree, which is demonstrated to achieve full frequency reliability with limited conservativeness. A modified IEEE 14-bus system has been used to conduct several case studies, assessing the effectiveness and the economic value of this system-aware control strategy for WTs. The results highlight the importance of dynamically optimising the value of the adaptive droop gain within the system scheduling algorithm.

Future work will extend the scheduling model to a stochastic framework, to consider the inherent uncertainty in wind generation. In addition, the optimal KE extraction should be studied in view of every WT location within a WF, analysing if wake effects have a significant impact on the control strategy. Furthermore, the CoI-based model calls for a

re-evaluation, i.e., the local frequency should be assessed for the purpose of designing local controllers for WFs providing frequency support.

REFERENCES

[1] *Zero Carbon Operation 2025*, Nat. Grid ESO, U.K., 2019.
[2] *Pathway to 2030 Holistic Network Design Summary Report*, Nat. Grid ESO, U.K., 2022.
[3] M. Dreidy, H. Mokhlis, and S. Mekhilef, "Inertia response and frequency control techniques for renewable energy sources: A review," *Renew. Sustain. Energy Rev.*, vol. 69, pp. 144–155, Mar. 2017.
[4] E. Muljadi, V. Gevorgian, M. Singh, and S. Santoso, "Understanding inertial and frequency response of wind power plants," in *Proc. IEEE Power Electron. Mach. Wind Appl.*, Jul. 2012, pp. 1–8.
[5] Z. Wu, W. Gao, T. Gao, W. Yan, H. Zhang, S. Yan, and X. Wang, "State-of-the-art review on frequency response of wind power plants in power systems," *J. Mod. Power Syst. Clean Energy*, vol. 6, no. 1, pp. 1–16, Jan. 2018.
[6] K. Liu, Y. Qu, H.-M. Kim, and H. Song, "Avoiding frequency second dip in power unreserved control during wind power rotational speed recovery," *IEEE Trans. Power Syst.*, vol. 33, no. 3, pp. 3097–3106, May 2018.
[7] Z. Chu, U. Markovic, G. Hug, and F. Teng, "Towards optimal system scheduling with synthetic inertia provision from wind turbines," *IEEE Trans. Power Syst.*, vol. 35, no. 5, pp. 4056–4066, Sep. 2020.
[8] J. Lee, G. Jang, E. Muljadi, F. Blaabjerg, Z. Chen, and Y. C. Kang, "Stable short-term frequency support using adaptive gains for a DFIG-based wind power plant," *IEEE Trans. Energy Convers.*, vol. 31, no. 3, pp. 1068–1079, Sep. 2016.
[9] A. B. Attya, J. L. Dominguez-Garcia, and O. Anaya-Lara, "A review on frequency support provision by wind power plants: Current and future challenges," *Renew. Sustain. Energy Rev.*, vol. 81, pp. 2071–2087, Jan. 2018.
[10] G. Xu and L. Xu, "Improved use of WT kinetic energy for system frequency support," *IET Renew. Power Gener.*, vol. 11, no. 8, pp. 1094–1100, Jun. 2017.
[11] D. Yang, M. Kang, E. Muljadi, W. Gao, J. Hong, J. Choi, and Y. Kang, "Short-term frequency response of a DFIG-based wind turbine generator for rapid frequency stabilization," *Energies*, vol. 10, no. 11, p. 1863, Nov. 2017.
[12] M. Kheshti, S. Lin, X. Zhao, L. Ding, M. Yin, and V. Terzija, "Gaussian distribution-based inertial control of wind turbine generators for fast frequency response in low inertia systems," *IEEE Trans. Sustain. Energy*, vol. 13, no. 3, pp. 1641–1653, Jul. 2022.
[13] J. Lee, E. Muljadi, P. Srensen, and Y. C. Kang, "Releasable kinetic energy-based inertial control of a DFIG wind power plant," *IEEE Trans. Sustain. Energy*, vol. 7, no. 1, pp. 279–288, Jan. 2016.
[14] Z. Chu, N. Zhang, and F. Teng, "Frequency-constrained resilient scheduling of microgrid: A distributionally robust approach," *IEEE Trans. Smart Grid*, vol. 12, no. 6, pp. 4914–4925, Nov. 2021.
[15] J. Van de Vyver, J. D. M. De Kooning, B. Meersman, L. Vandevelde, and T. L. Vandoorn, "Droop control as an alternative inertial response strategy for the synthetic inertia on wind turbines," *IEEE Trans. Power Syst.*, vol. 31, no. 2, pp. 1129–1138, Mar. 2016.
[16] L. Ruttledge and D. Flynn, "Emulated inertial response from wind turbines: Gain scheduling and resource coordination," *IEEE Trans. Power Syst.*, vol. 31, no. 5, pp. 3747–3755, Sep. 2016.
[17] F. Teng and G. Strbac, "Assessment of the role and value of frequency response support from wind plants," *IEEE Trans. Sustain. Energy*, vol. 7, no. 2, pp. 586–595, Apr. 2016.
[18] L. Badesa, F. Teng, and G. Strbac, "Simultaneous scheduling of multiple frequency services in stochastic unit commitment," *IEEE Trans. Power Syst.*, vol. 34, no. 5, pp. 3858–3868, Sep. 2019.
[19] L. Badesa, F. Teng, and G. Strbac, "Optimal portfolio of distinct frequency response services in low-inertia systems," *IEEE Trans. Power Syst.*, vol. 35, no. 6, pp. 4459–4469, Nov. 2020.
[20] M. Paturet, U. Markovic, S. Delikaraoglou, E. Vrettos, P. Aristidou, and G. Hug, "Stochastic unit commitment in low-inertia grids," *IEEE Trans. Power Syst.*, vol. 35, no. 5, pp. 3448–3458, Sep. 2020.
[21] Z. Zhang, E. Du, F. Teng, N. Zhang, and C. Kang, "Modeling frequency dynamics in unit commitment with a high share of renewable energy," *IEEE Trans. Power Syst.*, vol. 35, no. 6, pp. 4383–4395, Nov. 2020.
[22] F. Pérez-Illanes, E. Álvarez-Miranda, C. Rahmann, and C. Campos-Valdés, "Robust unit commitment including frequency stability constraints," *Energies*, vol. 9, no. 11, p. 957, Nov. 2016.
[23] S. M. Mousavi-Taghiabadi, M. Sedighizadeh, M. Zangiabadi, and A. S. Fini, "Integration of wind generation uncertainties into frequency dynamic constrained unit commitment considering reserve and plug in electric vehicles," *J. Cleaner Prod.*, vol. 276, Dec. 2020, Art. no. 124272.
[24] P. Rabbanifar and N. Amjady, "Frequency-constrained unit-commitment using analytical solutions for system frequency responses considering generator contingencies," *IET Gener., Transmiss. Distrib.*, vol. 14, no. 17, pp. 3548–3560, Sep. 2020.
[25] T. Ding, Z. Zeng, M. Qu, J. P. S. Catalão, and M. Shahidehpour, "Two-stage chance-constrained stochastic thermal unit commitment for optimal provision of virtual inertia in wind-storage systems," *IEEE Trans. Power Syst.*, vol. 36, no. 4, pp. 3520–3530, Jul. 2021.
[26] A. Mehrzad, M. Darmiani, Y. Mousavi, M. Shafie-Khah, and M. Aghamohammadi, "A review on data-driven security assessment of power systems: Trends and applications of artificial intelligence," *IEEE Access*, vol. 11, pp. 78671–78685, 2023.
[27] W. D. Oliveira, J. P. A. Vieira, U. H. Bezerra, D. A. Martins, and B. D. G. Rodrigues, "Power system security assessment for multiple contingencies using multiway decision tree," *Electr. Power Syst. Res.*, vol. 148, pp. 264–272, Jul. 2017.
[28] C. Liu, K. Sun, Z. H. Rather, Z. Chen, C. L. Bak, P. Thøgersen, and P. Lund, "A systematic approach for dynamic security assessment and the corresponding preventive control scheme based on decision trees," *IEEE Trans. Power Syst.*, vol. 29, no. 2, pp. 717–730, Mar. 2014.
[29] J. L. Cremer, I. Konstantelos, and G. Strbac, "From optimization-based machine learning to interpretable security rules for operation," *IEEE Trans. Power Syst.*, vol. 34, no. 5, pp. 3826–3836, Sep. 2019.
[30] Y. Zhang, C. Chen, G. Liu, T. Hong, and F. Qiu, "Approximating trajectory constraints with machine learning—Microgrid islanding with frequency constraints," *IEEE Trans. Power Syst.*, vol. 36, no. 2, pp. 1239–1249, Mar. 2021.
[31] A. Venzke and S. Chatzivasileiadis, "Verification of neural network behaviour: Formal guarantees for power system applications," *IEEE Trans. Smart Grid*, vol. 12, no. 1, pp. 383–397, Jan. 2021.
[32] Y. Du, F. Li, and C. Huang, "Applying deep convolutional neural network for fast security assessment with N-1 contingency," in *Proc. IEEE Power Energy Soc. Gen. Meeting (PESGM)*, Aug. 2019, pp. 1–5.
[33] M. Sun, I. Konstantelos, and G. Strbac, "A deep learning-based feature extraction framework for system security assessment," *IEEE Trans. Smart Grid*, vol. 10, no. 5, pp. 5007–5020, Sep. 2019.
[34] B. Tan, J. Yang, Y. Tang, S. Jiang, P. Xie, and W. Yuan, "A deep imbalanced learning framework for transient stability assessment of power system," *IEEE Access*, vol. 7, pp. 81759–81769, 2019.
[35] Rizwan-ul-Hassan, C. Li, and Y. Liu, "Online dynamic security assessment of wind integrated power system using SDAE with SVM ensemble boosting learner," *Int. J. Electr. Power Energy Syst.*, vol. 125, Feb. 2021, Art. no. 106429.
[36] B. Wang, B. Fang, Y. Wang, H. Liu, and Y. Liu, "Power system transient stability assessment based on big data and the core vector machine," *IEEE Trans. Smart Grid*, vol. 7, no. 5, pp. 2561–2570, Sep. 2016.
[37] M. Rajabdorri, E. Lobato, and L. Sigrist, "Robust frequency constrained UC using data driven logistic regression for island power systems," *IET Gener., Transmiss. Distrib.*, vol. 16, no. 24, pp. 5069–5083, Dec. 2022.
[38] D. T. Lagos and N. D. Hatziargyriou, "Data-driven frequency dynamic unit commitment for island systems with high RES penetration," *IEEE Trans. Power Syst.*, vol. 36, no. 5, pp. 4699–4711, Sep. 2021.
[39] S. Heier, *Grid Integration of Wind Energy: Onshore and Offshore Conversion Systems*. Hoboken, NJ, USA: Wiley, 2014.
[40] X. Zhao, Y. Xue, and X.-P. Zhang, "Fast frequency support from wind turbine systems by arresting frequency nadir close to settling frequency," *IEEE Open Access J. Power Energy*, vol. 7, pp. 191–202, 2020.
[41] S. El Itani, U. D. Annakkage, and G. Joos, "Short-term frequency support utilizing inertial response of DFIG wind turbines," in *Proc. IEEE Power Energy Soc. Gen. Meeting*, Jul. 2011, pp. 1–8.
[42] D. Bertsimas and J. Dunn, "Optimal classification trees," *Mach. Learn.*, vol. 106, no. 7, pp. 1039–1082, Jul. 2017.
[43] Y. Chen, Y. Li, J. Xiang, and X. Shen, "An optimal power flow formulation with SOCP relaxation in radial network," in *Proc. IEEE 14th Int. Conf. Control Autom. (ICCA)*, Jun. 2018, pp. 921–926.

[44] J. A. Taylor, *Convex Optimization of Power Systems*. Cambridge, U.K.: Cambridge Univ. Press, 2015.
[45] A. Dyśko, D. Tzelepis, and C. Booth, "Assessment of risks resulting from the adjustment of vector shift (VS) based loss of mains protection settings. Phase II," Univ. Strathclyde, U.K., Tech. Rep. NG/LOM/TR/2017-001A, 2017.
[46] R. D. Zimmerman, C. E. Murillo-Sánchez, and R. J. Thomas, "MATPOWER: Steady-state operations, planning, and analysis tools for power systems research and education," *IEEE Trans. Power Syst.*, vol. 26, no. 1, pp. 12–19, Feb. 2011.
[47] *PowerWorld*. Accessed: May 2024. [Online]. Available: https://www.powerworld.com
[48] E. Rakhshani and P. Rodriguez, "Inertia emulation in AC/DC interconnected power systems using derivative technique considering frequency measurement effects," *IEEE Trans. Power Syst.*, vol. 32, no. 5, pp. 3338–3351, Sep. 2017.
[49] L. Badesa, G. Strbac, M. Magill, and B. Stojkovska, "Ancillary services in great Britain during the COVID-19 lockdown: A glimpse of the carbon-free future," *Appl. Energy*, vol. 285, Mar. 2021, Art. no. 116500.
[50] J. Lofberg, "YALMIP: A toolbox for modeling and optimization in MATLAB," in *Proc. IEEE Int. Conf. Robot. Autom.*, Sep. 2004, pp. 284–289.

QIAN CHEN (Student Member, IEEE) received the joint B.Eng. degree in electrical and electronic engineering from Xi'an Jiaotong–Liverpool University, China, and the University of Liverpool, U.K., in 2019, and the M.Sc. degree in future power systems from Imperial College London, in 2020, where he is currently pursuing the Ph.D. degree. His research interests include power system operation and security.

LUIS BADESA (Member, IEEE) received the Ph.D. degree in electrical engineering from Imperial College London, U.K. He is currently an Associate Professor in electrical engineering with the School of Industrial Engineering and Design (ETSIDI), Technical University of Madrid (UPM), Spain. His research interests include the operation and economics of low-inertia electricity grids.

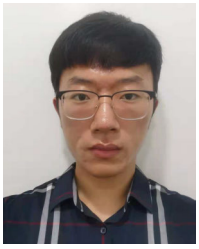

ZHONGDA CHU (Member, IEEE) received the M.Sc. degree in electrical engineering and information technology from the Swiss Federal Institute of Technology, Zürich, Switzerland, in 2018, and the Ph.D. degree in electrical engineering from Imperial College London, London, U.K., in 2022. He is currently a Research Associate with the Department of Electrical and Electronic Engineering, Imperial College London. His research interests include control and optimization of power systems with high power electronics penetration.

GORAN STRBAC (Member, IEEE) is currently a Professor of electrical energy systems with Imperial College London, U.K. His current research interests include the optimization of operation and investment of low-carbon energy systems, energy infrastructure reliability, and future energy markets.